Effects of O_2 on low-pressure CO-laser discharges

W. Lowell Morgan*
Department of Physics, University of Windsor, Windsor, Ontario, Canada
and Research Institute for Engineering Sciences, Wayne State University, Detroit, Michigan 48202

Edward R. Fisher
Department of Chemical Engineering and Research Institute for Engineering Sciences, Wayne State University, Detroit, Michigan 48202
(Received 10 February 1977)

Trace additions of several gases are known to significantly effect CO-laser power and efficiency. Since small concentrations of additives are generally involved, these additives are recognized as predominantly influencing the characteristics of the laser plasma. Oxygen has been an additive receiving substantial attention in past measurements. In this paper we develop a consistent interpretation for all the observed oxygen effects both from our laboratories and elsewhere. Oxygen in small concentrations will be shown to improve laser efficiency and power through its effect on the electron-ion recombination process. At higher oxygen additions, laser output is degraded as a result of vibrational-translation relaxation by oxygen atoms. In addition, carbon formation and removal, plasma heating and cooling effects, heterogeneous loss processes, and the influence of polymer ions will be discussed through model calculations.

I. INTRODUCTION

Oxygen as an additive in discharge-sustained CO molecular laser systems has been used extensively to improve laser output. Although numerous observations on the role of oxygen have been made, no consistent interpretation has been developed which characterizes these observations. In this paper we review the observations on oxygen as an additive and present a detailed model which provides a consistent framework for interpreting these observations as well as the effects of other additives in the CO-laser system.

In order to accomplish this understanding, the characteristics of the electron energy distribution have been studied through a numerical solution to the relevant Boltzmann equation, and the detailed plasma and neutral chemistry and energy transfer processes have been characterized through a time-dependent rate equation model. These models are detailed in this paper with application to the CO-O_2-He system. Two major points are indicated as a result of this study on the effect of oxygen on CO-laser performance: ionic and neutral chemistry are very important to an understanding of the observations on oxygen effects, and superelastic processes are critical to explaining observed ionization levels.

A uniform feature of additive gases found to enhance laser power and efficiency is the fact that these gases have lower ionization potentials than either CO or He. Thus, the additive can generally be viewed as being a source of electrons at an E/N [(electric field)/(total number density)] more appropriate to maintaining the mean electron energy near that for optimum coupling to the vibrational states of CO. Although this viewpoint is undoubtedly correct for some additives of general interest, e.g., Xe, oxygen will be shown to enhance laser output and efficiency as a result of its effect on the ion recombination dynamics in the plasma.

In this paper, homogeneous plasma chemistry and energy transfer processes will be stressed. At total pressures around 10 torr under liquid nitrogen cooling, it will be shown that ambipolar diffusion competes about equally with homogeneous recombination as the major electron-loss process. At higher pressures, the electron density is dominated by ionization and homogeneous recombination. Attachment processes will be shown to be generally unimportant due to the large detachment rate by CO.

II. ELECTRON ENERGY DISTRIBUTION CALCULATIONS

A. Electron impact cross-section data

A summary of the electron impact cross-section data used in this study appears in Table I. Special mention should be made of the cross sections for electronic excitation of CO. Near the threshold, there is little information on the magnitude of the cross section for electronic excitation in CO. Most previous workers have used a single composite cross section, due to Hake and Phelps,[1] with a threshold of 6 eV and a peak value of 5×10^{-16} cm^2 at 10 eV corresponding to the CO($a\,^3\Pi$) state. This cross section, however, is subject to considerable uncertainty as pointed out by Hake and Phelps.[1]

For total cross sections from threshold up to

TABLE I. Electron impact processes in the CO-O_2 system.

Electron impact processes	Energy loss (eV)	Reference
$e^- + CO$:		
1. $CO^\dagger$ (8 levels)[a]	0.266–2.034	2
2. $CO(a\,^3\Pi)$	6.04	see text
3. $CO(A\,^1\Pi)$	8.07	see text
4. $C + O^-$	9.00	3
5. $C^+ + O^-$	12.55	3
6. CO^+	14.013	4
$e^- + O_2$:		
7. $O_2^\dagger$ (8 levels)	0.193–1.46	4
8. $O_2(a\,^1\Delta_g)$	0.98	5
9. $O_2(b\,^1\Sigma_g^+)$	1.64	5
10. $O_2(A\,^3\Sigma_u^+)$	4.5	1,6
11. $O_2(B\,^3\Sigma_u^-)$	8.4	1,6
12. 9.7 eV allowed[9]	9.7	6
13. $O + O^-$	3.62	3
14. O_2^+	12.063	4
15. $O^+ + O$	19.54	3
$e^- + O$:		
16. $O(^1D)$	1.96	7
17. $O(^1S)$	4.17	7
18. O^+	13.6	4
$e^- + O_2^*$:		
19. O_2^+	11.0	see text

[a]The dagger (†) refers to vibrational excitation and the asterisk (*) refers to electronic excitation.

about 25 eV, the work of Ajello[8] on the excitation of $CO(a\,^3\Pi)$ and $CO(A\,^1\Pi)$ has been used together with the theoretical work of Chung and Lin[9] on the excitation of eleven CO electronic states. In the calculations reported here we have included the two CO electronic states with the largest cross sections: the $a\,^3\Pi$ state at 6.4 eV and the $A\,^1\Pi$ state at 8.07 eV. The cross sections used are composites of those given in Refs. 8 and 9. They are in substantial agreement with a similar set of cross sections due to Sawada *et al.*[10]

With reference to the excitation of the $A\,^3\Sigma$ and $B\,^3\Sigma$ states of O_2, it is known that these excited states predissociate. The $O_2(A\,^3\Sigma_u^+)$ state[11] predissociates into $O(^3P) + O(^3P)$ and $O_2(B\,^3\Sigma_u^-)$ predissociates into $O(^3P) + O(^1D)$.[11,12] Although there are several ways for the $O_2(B)$ state to predissociate into $O(^3P) + O(^3P)$ via curve crossings,[12] the probabilities of this occurring are unknown. It has been assumed in this work that all of the excitation follows the $^3P + {}^1D$ predissociative path. The cross section for ionization of the O_2* metastable is unknown and has been taken to be the same as that for ionization of $O_2(X)$ displaced in energy by the excitation energy of O_2*. This is about the least arbitrary method of obtaining an estimate of the cross section for this process in the absence of experimental or theoretical data. There is some support for this assumption from the work of Burrow[13] on dissociative attachment from O_2*. He measured the ratio of the ionization cross section of the $a\,^1\Delta_g$ state to that of the $X\,^3\Sigma_g$ state at approximately 0.5 eV above each respective threshold and found it to be 0.8 ± 0.3.

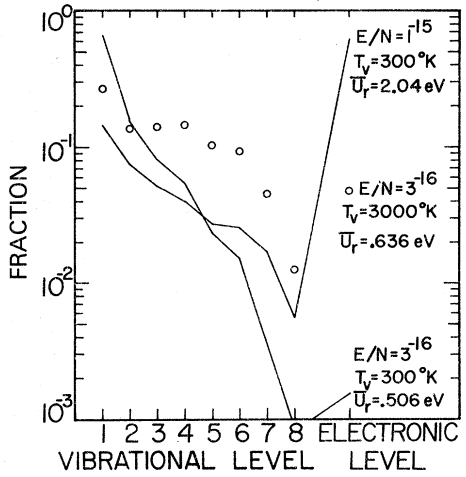

FIG. 1. Fractional energy balance in pure CO as a function of E/N. The effect of including superelastic processes is demonstrated by the circled points.

B. Results for CO

Nighan[14] has shown through electron energy distribution calculations that as the E/N of a discharge is increased, the fraction of energy going into electronic excitation of CO increases at the expense of vibrational excitation, suggesting that laser operation at low E/N is desirable. This is illustrated in Fig. 1 which plots the fraction of electron energy going into the CO vibrational and electronics states for two values of E/N. Here $\bar{u}_r = 2/3\bar{u}$, where $\bar{u}$ is the mean electron energy. The effect of superelastic collisions with vibrationally excited CO is also shown in the Fig. 1. Electrons in the 1–4-eV energy range gain quanta of energy from the excited vibrational states, ranging from 0.27 eV for $v=1$ to 2.30 eV for $v=8$, increasing the mean energy of the distribution. This has only a slight effect on the vibrational excitation rate coefficients, but dominates the electronic excitation and ionization rate coefficients due to the significant increase in the number of electrons in the high-energy tail of the distribution function. This superelastic feedback will be shown later to be of great importance in CO-laser operation.

III. CO-O_2-He DISCHARGE

A. Review of experimental work on the effects of O_2 on the CO laser

A number of experimenters[15–19] have found that a small amount of O_2 added to a cw CO-laser plasma has a pronounced effect upon the operation of the laser. Bhaumik *et al.*[16] have found that small amounts of O_2 (approximately 5% of the CO partial pressure) enhanced the power output by a factor of 10–20% and reduced carbon deposits on the walls of the laser tube. They suggested that the O_2 affected the dissociation reaction $CO \rightleftharpoons C + O$ by driving it to the left. Larger amounts of O_2 had a deleterious effect on laser operation, possibly, in their opinion, due to the large electron attachment cross section of O_2 or to the formation of CO_2. Hartwick and Walder[17] found that the total laser output increased and that the laser became more stable with the addition of O_2 to the CO-He discharge. The optimum mixture was found to be 28 torr He, 2 torr CO and 0.1 torr O_2. In addition, they measured the gas temperature in the plasma using a thermocouple and correlated it to laser output, finding that the minimum in temperature, approximately 295 °K, corresponded to the maximum in power output as the O_2 flow rate was varied for a liquid-nitrogen-cooled laser. At slow oxygen flow rates the measured kinetic temperature was approximately 320 °K.

Extensive work involving the effects of O_2 upon CO lasers has been done by Keren, Avivi, and Dothan.[18,19] They found that the addition of O_2 increased the power output and decreased the operating E/N of a water-cooled CO flow laser. At a constant current of 17 mA the laser output power reached a maximum of 4 W with the addition of 50 mtorr of O_2 to a mixture of 1.4 torr CO in 18 torr He and the axial field strength in the discharge dropped from 136 to 88 V/cm. Power output then decreased with the addition of larger concentrations of O_2 and lasing was completely quenched at an O_2 partial pressure of 100 mtorr. They also pointed out that the discharge was very unstable and that laser action could not be obtained in the absence of the O_2 additive. On the basis of the measured decrease in E/N and a calculation of the fraction of electron energy flowing into CO vibrational and electronic states as a function of E/N (similar to that presented in Fig. 1 here), they concluded that the enhanced power output was due to more efficient vibrational pumping because of the lower E/N.

Keren *et al.*[19] also analyzed the composition of the ions leaving the discharge using a mass spectrometer and found that with the addition of 20 mtorr O_2 to the laser plasma (1.4% of the CO partial pressure), O_2^+ became the dominant positive ion in the discharge. With no oxygen present the discharge was dominated by the $C_2O_2^+$ dimer ion and higher-order polymer ions. They suggested that the dominance of O_2^+ was due to ionization via a three-step process:

$$e^- + CO \rightarrow CO^*(a^3) + e^-,$$

$$CO^* + O_2 \rightarrow CO + O_2^*(\text{metastable}),$$

$$O_2^* + e^- \rightarrow O_2^+ + 2e^-,$$

claiming that the probability of producing O_2^+ by direct ionization is at least a factor of 20 lower than the probability of the above process. They dismiss the charge transfer reaction

$$CO^+ + O_2 \rightarrow O_2^+ + CO$$

as a means of forming O_2^+ because, in their opinion, it cannot explain the decrease in E/N that occurs with the addition of molecular oxygen. Using this three-step model, they compute that about 5% of the O_2 molecules are excited to O_2^* for a total O_2 partial pressure of 25 mtorr.

Because very small amounts of molecular oxygen added to a CO laser have significant effects upon laser performance, it appears clear that the plasma properties of the discharge are affected, but, until now, a consistent interpretation has not been available. The calculations that follow are directed toward providing this systematic explanation of the observed properties of additive O_2 in a CO discharge.

B. Plasma chemistry calculations

In order to assess the importance of some of the processes that can occur in the discharge, the computer code for calculating the electron distribution function[20] was combined with a time-dependent chemical kinetics code. This allows the concentrations of all important chemical species to be computed as a function of time. Since we are studying cw laser behavior, this computation is carried out for times of the order of contact times in flowing cw laser systems (i.e., tenths of seconds). On these time scales many of the species concentrations are in steady state. The differential rate equations are integrated directly rather than solving the steady-state equations because the coupled nonlinear algebraic equations that arise from a steady-state analysis are difficult to solve in a systematic way. More importantly, there are some species in a fast flow laser (such as CO_2 in a CO laser) that may not reach steady state. The chemistry code that was used in this work is based on the Runge-Kutta-Merson algorithm for the integration of stiff differential equations originally developed by Keneshea[21] in his studies of ionispheric chemistry. In this scheme, initial CO, O_2, and He densities and an initial electron and ion density close to their expected steady-state values are specified. A value for E/N and an initial vibrational temperature are also specified as inputs to the calculation of the electron energy distribution. As time progresses and the CO vibrational temperature changes, the electron distribution function is recomputed and new rate coefficients calculated to reflect these changes.

A list of the 79 chemical reactions included in this calculation is presented in Table II. Only a relative few, however, are really important and will be discussed here. The rate coefficients for the reactions and references to them are also given in Table II. The rate coefficients for the first 20 reactions, except number (8), are computed using the electron energy distribution code and the cross sections discussed above. The rate coefficient used for ionization of vibrationally excited CO [reaction (8)] is taken to be the same as that for ionization of ground-state CO [reaction (5)]. The rate coefficients shown in Table II for reactions (1) through (20) were computed using an $E/N = 1 \times 10^{-16}$ V cm^2 and a CO vibrational temperature of 3000 °K for a gas mixture corresponding to 1.4 torr CO, 50 mtorr O_2, and 18 torr He. These values are shown for illustrative purposes as they are typical of the conditions being discussed in this work. The electron reduced mean energy ($\bar{u}_r$) under these conditions is about 1.0 eV. The gas temperature has been taken to be 300 °K. The rate coefficients in reactions (21) through (79), where they are dependent upon electron or gas temperature, have been computed using these values.

To illustrate how the parameters critical to the calculations being presented here vary with E/N and vibrational temperatures, we have, in Figs. 2–4 plots of the ionization rate coefficient of CO, mean electron energy, and CO^+, $C_2O_2^+$, and O_2^+ recombination rate coefficients. These were com-

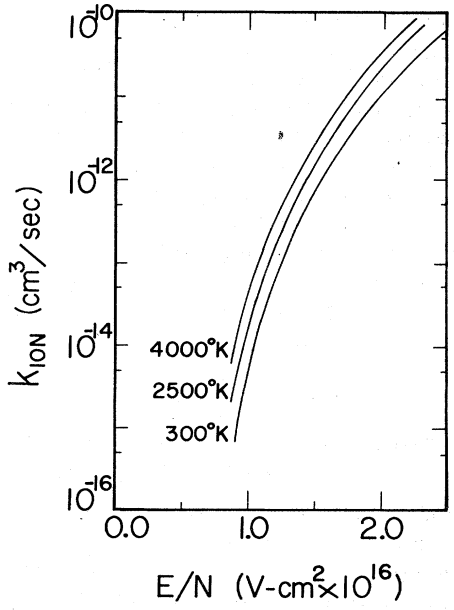

FIG. 2. CO ionization rate coefficients for a 7% CO–93% He mixture as a function of CO vibrational temperature.

TABLE II. Reactions included in the plasma chemistry calculations. The notation 3.8 (–12) means 3.8×10^{-12} cm^3/molecule sec. Also, the dagger (†) refers to vibrational excitation while the asterisk (*) refers to electronic excitation.

No.	Reactions	k	References
1.	$CO + e = CO^{\dagger} + e$	9.4 (–9)	
2.	$CO^{\dagger} + e = CO + e$	2.2 (–8)	
3.	$CO + e = CO^{*} + e$	6.8 (–11)	
4.	$CO^{*} + e = CO + e$	1.6 (–8)	
5.	$CO + e = CO^{+} + e + e$	2.4 (–14)	
6.	$CO + e = C + O^{-}$	2.8 (–14)	
7.	$CO + e = C^{+} + O^{-} + e$	9.3 (–17)	
8.	$CO^{\dagger} + e = CO^{+} + e + e$	2.4 (–14)	
9.	$O_2 + e = O_2^{\dagger} + e$	2.3 (–10)	
10.	$O_2^{\dagger} + e = O_2 + e$	4.2 (–10)	
11.	$O_2 + e = O_2^{*} + e$	1.9 (–10)	
12.	$O_2^{*} + e = O_2 + e$	5.4 (–10)	
13.	$O_2 + e = O_2^{+} + e + e$	6.6 (–14)	
14.	$O_2 + e = O + O + e$	5.1 (–11)	
15.	$O_2 + e = O + O^{-}$	5.5 (–12)	
16.	$O_2 + e = O^{+} + O^{-} + e$	6.1 (–18)	
17.	$O_2 + e = O + O^{*} + e$	2.6 (–11)	
18.	$O + e = O^{*} + e$	6.1 (–10)	
19.	$O + e = O^{+} + e + e$	4.9 (–14)	
20.	$O_2^{*} + e = O_2^{+} + e + e$	1.6 (–13)	
21.	$O^{-} + CO = CO_2 + e$	7.3 (–10)	22
22.	$CO^{*} + CO = CO^{\dagger} + CO^{\dagger}$	9.9 (–11)	23
23.	$CO^{*} + CO = C + CO_2$	1.1 (–11)	23
24.	$CO^{+} + CO + CO = C_2O_2^{+} + CO$	1.4 (–28)	24–27
25.	$C_2O_2^{+} + CO = CO^{+} + CO + CO$	2.1 (–12)	24–27
26.	$C_2O_2^{+} + e = CO + CO$	7.4 (–8)	28
27.	$O_2^{+} + e = O + O$	1.0 (–8)	29
28.	$O_2^{+} + e = O + O^{*}$	1.0 (–8)	29
29.	$O^{*} + O_2 = O + O_2$	7.5 (–11)	30
30.	$O_2 + O + M = O_3 + M$	6.4 (–34)	31
31.	$O^{*} + O_3 = O_2 + O_2$	3.8 (–12)	30
32.	$O + O_3 = O_2 + O_2$	2.0 (–14)	31
33.	$O_2 + O_3 = O_2 + O_2 + O$	1.5 (–13)	31
34.	$O^{+} + O_2 = O_2^{+} + O$	4.0 (–11)	32
35.	$O_2^{+} + e + M = O_2 + M$	8.0 (–29)	21
36.	$O^{-} + O_2^{+} = O + O_2$	1.0 (–7)	33
37.	$O^{-} + O = O_2 + e$	2.0 (–10)	33
38.	$O^{-} + O_2 = O_3 + e$	5.0 (–15)	33
39.	$O_3 + e = O^{-} + O_2$	1.0 (–11)	33

TABLE II. (*Continued*)

No.	Reactions	k	References
40.	$O^- + O_2^* = O_3 + e$	3.0 (–10)	33
41.	$O^- + O_2^+ + M = O_3 + M$	1.9 (–27)	est.
42.	$O_2 + e + M = O_2^- + M$	1.0 (–33)	34
43.	$O + e + M = O^- + M$	1.0 (–31)	21
44.	$C + O_2 = CO^\dagger + O^*$	3.3 (–11)	35
45.	$C + CO_2 = CO + CO$	7.0 (–19)	35
46.	$C + O_2^+ = CO^+ + O$	2.3 (–10)	35
47.	$C^+ + CO_2 = CO^+ + CO$	1.8 (–9)	32
48.	$C^+ + O_2 = CO^+ + O$	1.1 (–9)	32
49.	$CO^+ + e = C + O$	9.2 (–8)	35
50.	$CO^+ + e + M = CO + M$	8.5 (–27)	33
51.	$C + O + M = CO + M$	1.0 (–32)	35
52.	$CO^+ + O_2 = CO + O_2^+$	2.0 (–10)	32
53.	$CO^+ + O = CO + O^+$	1.4 (–10)	33
54.	$C_2O_2^+ + O_2 = CO + CO + O_2^+$	2.0 (–10)	est.
55.	$O^+ + CO_2 = O_2^+ + CO$	1.1 (–9)	33
56.	$CO^* + O_2 = CO + O_2^*$	2.0 (–10)	23
57.	$O^* + CO = O + CO^\dagger$	1.7 (–11)	36
58.	$O^* + CO = O + CO$	5.6 (–11)	36
59.	$O + CO^\dagger = O + CO$	5.9 (–15)	37
60.	$O_2^- + O = O_3 + e$	5.0 (–10)	32
61.	$O_2^- + O = O_2 + O^-$	3.3 (–10)	33
62.	$O_2^- + O_2^+ = O_2 + O_2$	4.2 (–7)	33
63.	$O_2^- + O_2 = O_2 + O_2 + e$	2.0 (–18)	33
64.	$O_2^- + O_3 = O_2 + O_3^-$	4.0 (–10)	33
65.	$O_2^- + O_2^* = O_2 + O_2 + e$	2.0 (–10)	33
66.	$O^- + O_3 = O + O_3^-$	1.0 (–9)	33
67.	$O_2^+ + O_3^- = O_3 + O + O$	1.0 (–7)	38
68.	$O_2^+ + O_3^- = O_3 + O_2$	2.0 (–7)	38
69.	$O_3^- + O = O_2^- + O_2$	1.0 (–10)	38
70.	$O_3^- + O = O_2 + O_2 + e$	1.0 (–13)	38
71.	$O_2^+ + O_2 + O_2 = O_4^+ + O_2$	2.8 (–30)	33
72.	$O_2^+ + O_2 + M = O_4^+ + M$	1.0 (–31)	33
73.	$O_4^+ + O_2 = O_2^+ + O_2 + O_2$	2.0 (–13)	33
74.	$O_4^+ + O = O_2^+ + O_3$	3.0 (–10)	33
75.	$CO^\dagger + He = CO + He$	1.7 (–17)	39
76.	$CO^\dagger = CO + h\nu$	3.4 (+1)	40
77.	$O_2^\dagger + He = O_2 + He$	1.6 (–15)	41
78.	$O_4^+ + e = O_2 + O_2$	1.1 (–7)	29
79.	$O^+ + e + M = 0 + M$	2.0 (–27)	33

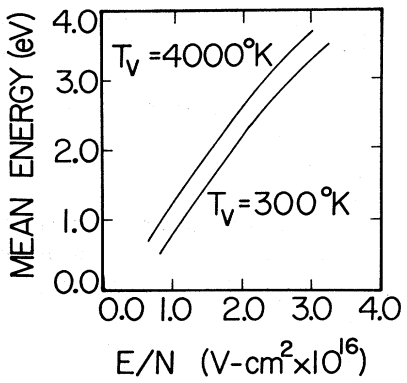

FIG. 3. Mean electron energy as a function of E/N and CO vibrational temperature for a mixture of 7% CO-93% He.

puted for mixtures of 1.4 torr CO, 50 mtorr O_2, and 18 torr He corresponding to the experimental conditions of Keren *et al.*[18,19] The rate coefficient for recombination of $C_2O_2^+$ was obtained from Center,[28] who assumed that in his high-pressure experiments the dominant ion was $C_2O_2^+$ or a higher-order polymer ion.

The results of the calculation of the time evolution of chemical species in a CO-O_2-He discharge are displayed in Figs. 5–8. In these calculations, the electron density was taken to be 5×10^9 cm^{-3} initially, with a gas mixture of 1.4 torr CO, 50μ O_2, and 18 torr He and E/N equal to 1.05×10^{-16} V cm^2. The initial CO vibrational temperature was chosen to be 1000 °K and, as it increased, the electron impact rate coefficients were recomputed at T_{vib} = 1500, 2000, 2400 °K, etc. The species CO, O_2, O, O_2*, and He were included in the calculation of the electron energy distribution function, but the presence of oxygen in small concentrations has little effect upon the shape of the distribution function even in the high-energy

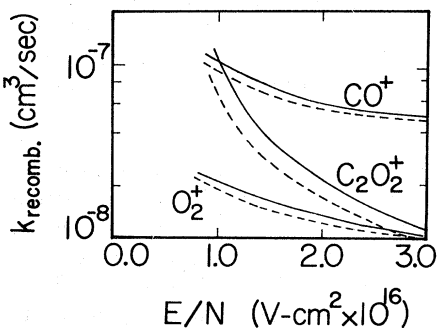

FIG. 4. Recombination rate coefficients as a function of E/N for two CO vibrational temperatures (solid line is 300 °K; dotted line is 4000 °K).

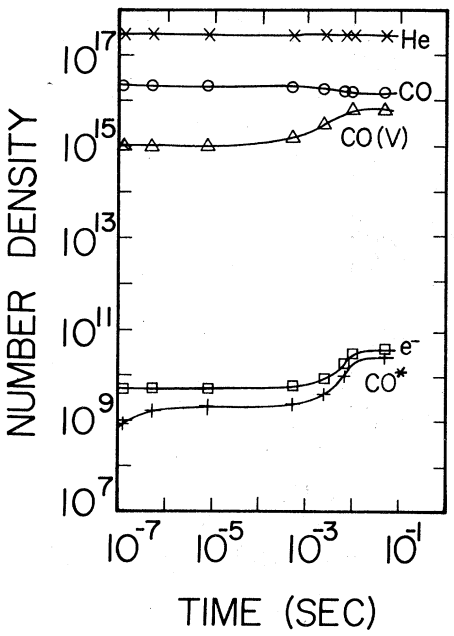

FIG. 5. CO-O_2-He kinetics at 300 °K for a mixture ratio 0.072-0.0026-0.9254 at 19.5 torr.

tail.

The above calculations show that O_2^+ becomes the dominant ion in CO lasers containing O_2 due to charge transfer reactions and that, as a consequence of recombination kinetics, it is respon-

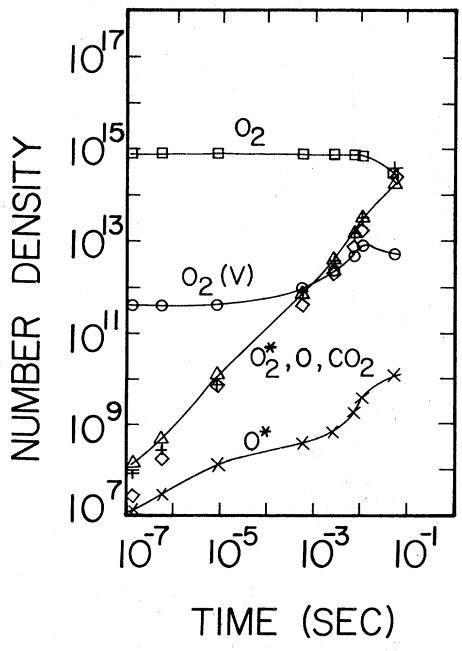

FIG. 6. CO-O_2-He kinetics (a continuation of Fig. 5).

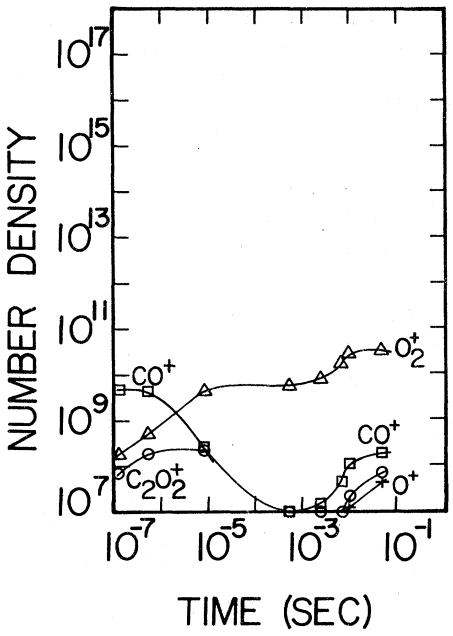

FIG. 7. $CO-O_2$-He kinetics (a continuation of Fig. 6).

sible for the lowering of the E/N in a current regulated discharge. This is in direct opposition to the explanation advanced by Keren *et al.*[18,19] This lowering of E/N allows for more efficient pumping of the CO vibrational levels as well as reduced plasma heating as a result of electronic excitation

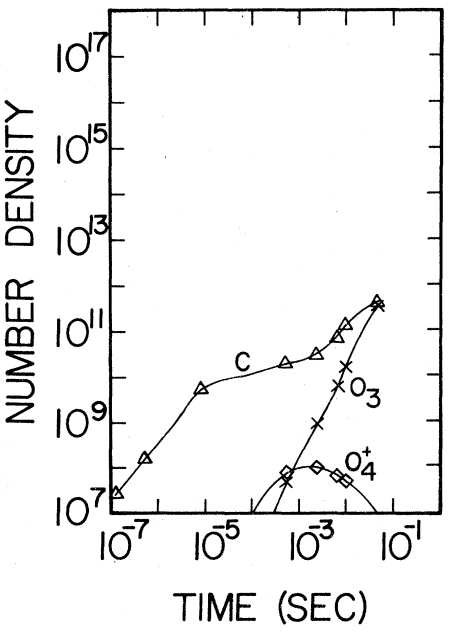

FIG. 8. $CO-O_2$-He kinetics (a continuation of Fig. 7). Note that O_2^-, O^-, C^+, O_3^- have densities below $10^{-7}/cm^3$

of CO followed by rapid quenching. Both factors lead to increased power output. The calculations also demonstrate that O atoms, formed predominantly by electron impact dissociation of O_2, have an adverse effect upon laser performance when O_2 is added in large enough concentrations. This is due to relaxation of the CO laser levels by vibrational translational energy exchange in CO-O collisions. The details of these findings and others are presented in the following sections.

IV. RESULTS

A. Ion kinetics of the $CO-O_2$-He discharge

It was pointed out above that O_2^+ is found[19] to be the dominant positive ion in CO discharges containing oxygen, even when the O_2 is present in partial fractions less than 1%. The results of the calculation (Fig. 7) are in agreement with this observation. The dominance of O_2^+ is due to O_2 having the lowest ionization potential of the major species in the discharge and is formed almost entirely through charge transfer reactions. $C_2O_2^+$, which is the dominant ion in CO discharges without oxygen, and CO^+ both readily charge transfer with O_2 [reaction (54)].

Ionization from the O_2 metastable, which appears in large concentrations due to reactions (11) and (56),

$$O_2 + e^- \rightarrow O_2^* + e^-, \tag{11}$$

$$CO^* + O_2 \rightarrow CO + O_2^*, \tag{56}$$

has been included in these calculations, but is unimportant as a source of O_2^+ in comparison to the charge transfer process. The relative rates of O_2^* ionization and CO ionization for typical cw flow laser contact time of 0.1 sec are shown in Table III. By reference to Table III we see that the direct ionization of CO [reaction (5)] is over an order of magnitude larger than the ionization rate of metastable O_2^+ [reaction (20)]. This observation is in disagreement with Keren *et al.*[18,19] who postulated that ionization via metastable O_2 is the dominant process for O_2^+ production.

This replacement of CO^+ and $C_2O_2^+$ by O_2^+ as the major ionic species has an important effect upon the voltage-current characteristics of the discharge. For simplicity, if one assumes that the only formation and removal processes for electrons are ionization and homogeneous recombination, respectively, the electrons are in a steady-state density which can be computed from (recognizing that O_2^+, CO^+, and $C_2O_2^+$ recombine through a two-body process at the pressures of interest here)

$$\frac{d[e^-]}{dt} = k_{ion}[e^-][CO] - k_{recomb}[e^-][ion^+].$$

TABLE III. Rate constants and rates of individual reactions at $t = 0.1$ sec using the reactions in Table II.

	k	Rate		k	Rate
1.	9.22 (–9),	5.36 (18)	41.	1.90 (–27),	8.53 (7)
2.	2.24 (–8),	5.19 (18)	42.	1.00 (–33),	1.52 (9)
3.	7.67 (–11),	4.46 (16)	43.	1.00 (–31),	7.15 (11)
4.	1.57 (–8),	1.47 (13)	44.	3.30 (–11),	4.38 (15)
5.	2.98 (–14),	1.73 (13)	45.	6.98 (–19),	2.23 (8)
6.	3.29 (–14),	1.91 (13)	46.	2.30 (–10),	7.87 (12)
7.	1.12 (–16),	6.50 (10)	47.	1.80 (–9),	5.42 (10)
8.	2.98 (–14),	6.90 (12)	48.	1.10 (–9),	1.08 (10)
9.	2.35 (–10),	1.16 (15)	49.	9.20 (–8),	8.05 (11)
10.	4.16 (–10),	3.94 (13)	50.	8.40 (–27),	2.25 (10)
11.	1.88 (–10),	9.35 (14)	51.	1.00 (–32),	1.91 (12)
12.	5.44 (–10),	2.93 (15)	52.	2.00 (–10),	1.08 (10)
13.	8.02 (–14),	3.98 (11)	53.	1.40 (–10),	2.10 (13)
14.	5.51 (–11),	2.73 (14)	54.	2.00 (–10),	3.61 (12)
15.	5.97 (–12),	2.93 (13)	55.	1.10 (–9),	2.21 (13)
16.	7.46 (–18),	3.70 (7)	56.	2.00 (–10),	6.82 (14)
17.	2.99 (–11),	1.48 (14)	57.	1.72 (–11),	4.42 (15)
18.	6.16 (–10),	1.44 (16)	58.	5.58 (–11),	1.43 (16)
19.	5.97 (–14),	1.39 (12)	59.	5.90 (–15),	2.34 (16)
20.	1.90 (–13),	1.03 (12)	60.	5.00 (–10),	1.83 (9)
21.	7.30 (–10),	4.87 (13)	61.	3.28 (–10),	1.20 (9)
22.	9.90 (–8),	3.95 (16)	62.	4.20 (–7),	8.42 (7)
23.	1.10 (–11),	4.39 (15)	63.	2.00 (–18),	1.56 (0)
24.	1.43 (–28),	8.42 (12)	64.	4.00 (–10),	1.12 (6)
25.	2.10 (–12),	4.44 (12)	65.	2.00 (–10),	1.69 (8)
26.	7.32 (–8),	3.62 (11)	66.	1.00 (–9),	2.05 (9)
27.	1.01 (–8),	1.30 (13)	67.	1.00 (–7),	9.67 (7)
28.	1.01 (–8),	1.30 (13)	68.	2.00 (–7),	1.93 (8)
29.	7.50 (–11),	1.64 (14)	69.	1.00 (–10),	1.76 (9)
30.	6.43 (–34),	1.67 (13)	70.	1.00 (–13),	1.76 (6)
31.	3.80 (–12),	3.01 (10)	71.	2.80 (–30),	1.75 (9)
32.	2.00 (–14),	6.14 (12)	72.	1.00 (–31),	1.43 (11)
33.	1.50 (–13),	9.79 (12)	73.	2.00 (–13),	2.00 (7)
34.	4.00 (–11),	2.64 (11)	74.	3.00 (–10),	1.41 (11)
35.	8.00 (–29),	3.13 (10)	75.	1.70 (–17),	3.09 (16)
36.	1.00 (–7),	1.47 (10)	76.	3.36 (+1),	2.11 (17)
37.	2.00 (–10),	5.35 (11)	77.	1.60 (–15),	1.19 (15)
38.	5.00 (–15),	2.84 (6)	78.	1.11 (–7),	3.05 (9)
39.	1.00 (–11),	1.79 (11)	79.	2.00 (–27),	1.11 (9)
40.	3.00 (–10),	1.86 (11)			

If the ion and electron densities are assumed to be equal (i.e., one ion dominates and negative ions are unimportant) at steady state,

$$\frac{d[e^-]}{dt} = 0 \rightarrow [e^-]_{ss} = \frac{k_{\text{ion}}}{k_{\text{recomb}}}[\text{CO}].$$

As can be seen in Fig. 4, the rate coefficient for recombination of O_2^+ is substantially smaller than that of either CO^+ or $C_2O_2^+$. This results in an increased electron density when O_2^+ dominates so that, under constant current operation, the electric field must be reduced. A lower electric field increases the efficiency of electron impact excitation of the CO vibrational states as well as reducing the electron energy channeling into electronic excitation and hence heat, eventually resulting in increased power output.

As a test of this hypothesis, a simple model calculation was performed in which, given the recombination rate coefficient (as a function of electron temperature), E/N and CO vibrational temperatures were varied and the ionization rate coefficient calculated in order to achieve a chosen current density. Current density j (A/cm^2) is related to electron drift velocity v_d (cm/sec) and number density N_e (cm^{-3}) by

$$j = ev_dN_e,$$

where $e = 1.6 \times 10^{-19}$ C and where the drift velocity v_d can be computed from the electron energy distribution function.

If a similar steady-state analysis is carried out for excitation of CO($v = 1$) by electrons and deexcitation by superelastic collisions with electrons, which is predicted (see Table III) to be one of the major loss processes for low vibrational levels, we find at steady state,

$$\frac{[\text{CO}(v=1)]}{[\text{CO}(v=0)]} = \frac{k_{0\rightarrow 1}}{k_{1\rightarrow 0}}.$$

Using these two expressions and the equation for current density, we can choose an E/N and CO vibrational temperature, solve the Boltzmann equation obtaining rate coefficients, temperature, and drift velocity, and calculate a current density and new vibrational temperature. This process can be repeated until the assumed and computed vibrational temperatures are equal and the desired current density has been obtained. This approach is simple, but contains the essence of the processes involved in establishing the electron density in the plasma. The greatest inaccuracy lies in the assumption concerning vibrational excitation and deexcitation of CO($v = 1$) since there are other important processes, such as excitation and deexcitation to and from CO($v = 2, 3, \ldots$) that affect the population of the $v = 1$ level.

Despite its defects, this calculation gives results reasonable enough to illustrate the point concerning the relationship between recombination rate, E/N, and efficiency of vibrational excitation. The results are presented in Table IV. To achieve similar current densities and vibrational temperatures using the O_2^+ recombination coefficient required a 10% decrease in E/N from the value needed using the recombination coefficient for CO^+. The lowering of E/N resulted in a 34% decrease in the fraction of energy flowing into CO electronic states and a 9% increase in the fraction being channeled into $v = 1$ alone. Thus, in contrast to Keren *et al.*, we have shown that O_2^+ directly affects both the E/N of the plasma and

TABLE IV. Results of the simplified calculation of ionization-recombination processes.

	E/N (V cm^2)	$[e^-]$ (cm^{-3})	j (A/cm^2)	$\bar{\epsilon}$ (eV)	v_{drift} (cm/sec)	$f(CO^*)$	$f(CO_{v=1})$
Using k_{CO^+}	1.12×10^{-16}	$4.93\times10^{+10}$	23.4×10^{-3}	1.27	$2.97\times10^{+6}$	21.3%	18.1%
Using $k_{O_2^+}$	1.01×10^{-16}	$4.99\times10^{+10}$	22.2×10^{-3}	1.09	$2.78\times10^{+6}$	14.0%	19.8%

the excitation of CO vibrational energy, in agreement with the experimental observations.

B. Negative ions in a CO discharge

The time development of the negative ion densities is shown in Fig. 8. Although O^- is rapidly formed by dissociative attachment of CO and O_2 [reactions (6) and (15)], it is rapidly removed by detachment collisions with CO [reaction (21)]. This is in contrast to the chemistry of CO_2 lasers as discussed by Nighan and Wiegand[42] and by Garscadden and his collaborators,[43,44] where negative ions appear to control the stability of the discharge at low E/N. The results obtained here are consistent with the observations[42] that additions of CO to CO_2 lasers stabilize the discharge through electron detachment reactions with the negative ion species.

In order for attachment to $Fe(CO)_5$ impurity to be important as pointed out by Center,[28] the impurity level would have to be greater than 145 ppm. This level is substantially above the maximum level found by Center in his experiments; therefore, we expect that impurity attachment is not important to the conclusions reached in this study.

C. Role of atomic oxygen in the discharge

As mentioned earlier in this section, at higher O_2 partial pressures, the laser output power is found to decrease and the neutral temperature increase. Our calculations indicate that both of these effects are due to the formation of O atoms in the plasma. The cross sections for electron impact excitation of predissociative O_2 electronic states are large. This leads to a large production of oxygen atoms [reactions (14) and (17)] and a build-up in the O atom concentration in the discharge. The calculated time development of the several neutral oxygen species is shown in Fig. 6.

For very small concentrations of O_2 as an additive to CO lasers, the dissociation into O atoms has little effect upon laser performance. Above some threshold O_2 concentration, the O atom density increases to a level where vibrational-translational (VT) energy transfer collisions between CO and O [reaction (59)] is predicted to become the dominant deexcitation mechanism among the CO vibrational levels responsible for laser action. Since it is the higher vibrational levels that dominate the laser output spectrum, the presence of O atoms will degrade the laser output. A sample of available vibrational deexcitation rate coefficients for $CO(v=1)$ and $CO(v=12)$ are shown in Table V. For the low vibrational states ($v=1$ to $v\simeq 8$) superelastic collisions with electrons is the primary deexcitation process. In the absence of oxygen, radiation [reaction (76)] and VT collisions with He [reaction (75)] are primarily responsible for CO vibrational deexcitation. The radiative rate for $CO(v=12)$ molecule is given by the Einstein A coefficient in Table IV. The deactivation rate for $CO(v=12)$ by collision with He is $k_{VT}[He]=262$ sec^{-1} for 18 torr of He. This is approximately the same as the radiation rate. Using a superelastic rate coefficient for the $v=12\rightarrow 11$ transition equal to that for the $v=1\rightarrow 0$ and an electron density of 10^{10} gives a deexcitation rate of 10–100 sec^{-1}. Hence, radiation and He VT exchange are likely to be the dominant deexcitation

TABLE V. Deexcitation of CO vibrational levels.

	$v=1\rightarrow0$	$v=12\rightarrow11$
Radiation[40] $A=$	33.6 sec^{-1}	239.9 sec^{-1}
VT with He,[39] $k=$ ($T_{gas}=300$ °K)	1.7×10^{-17} cm^3/sec	9.0×10^{-16} cm^3/sec
VT with O,[37] $k=$	5.9×10^{-15} cm^3/sec	$\gtrsim2.9\times10^{-13}$ [a] cm^3/sec
VT with O_2,[48] $k=$		2.1×10^{-14} cm^3/sec
VT with CO_2,[48] $k=$		8.6×10^{-14} cm^3/sec
Superelastic $k=$ with e,	$10^{-9}-10^{-8}$ [b] cm^3/sec	

[a] The value shown is computed assuming the same scaling with v as the CO-He VT process.
[b] The rate coefficient is typically in this range with its exact value depending upon the electron energy distribution function.

mechanisms.

However, when O atoms are present, even in small concentrations, this may strongly affect vibrational relaxation since the CO-O VT rate coefficient for the lowest vibrational levels is more than 100 times larger than that for CO-He.[45] If the same scaling with v is assumed for VT relaxation by O atoms as exists for the He VT process (a substantial underestimate based on SSH[45] mass effect), an O atom partial pressure of only 52 mtorr would be needed for CO-O VT to be equal to the radiation or the CO-He VT process. Laser performance will be degraded when the contribution of the CO-O VT rates is non-negligible in comparison to the fixed radiation and CO-He VT rates. The scaling of vibrational rate coefficients with increasing vibrational level is, in general, uncertain. However, the collision system of $O(^3P)+CO(^1\Sigma,v')$, which correlates with the triplet state of CO_2, offers the possibility of a strong "chemical" interaction through curve crossing to the $CO_2(^1\Sigma)$ state and enhanced energy transfer possibilities associated with a short-lived triatomic complex.

Although the above arguments are somewhat qualitative due to a lack of reliable rate constant data information, our chemistry calculations predict substantial dissociation, up to 20%, for time scales of the order of flow contact times in typical CO lasers. For dissociation levels of this order, O atoms VT processes will substantially reduce the vibrational content of CO, leading to reduced laser output as well as increased plasma heating.

The effect of higher O_2 additions on the shape of the experimentally observed CO vibrational distribution up to $v \cong 30$ also clearly shows the emergence of a strong VT process, attributable to O atoms.[45,46]

It can be seen from the rate coefficients in Table V that vibrational relaxation by O_2 will be unimportant for the concentrations being discussed here. The same will be true for small concentrations of CO_2, which is formed primarily by reactions (21) and (23):

$$O^- + CO \rightarrow CO_2 + e^-, \tag{21}$$

$$CO^* + CO \rightarrow C + CO_2. \tag{23}$$

The density of CO_2 is still increasing, however (Fig. 7), at the end of the calculation indicating that there may be a large buildup of this species in closed CO systems. In flowing discharges with a residence time of 0.1–0.5 sec this may not be a problem, but in a sealed system, CO_2 may be present in large enough concentrations to be a major source of vibrational deexcitation.

D. Additional discussion of CO laser chemistry

We propose that carbon in the CO laser is formed primarily as a product in the quenching of electronically excited CO, i.e., reaction (23). Reactions (22) and (23),

$$CO^* + CO \rightarrow CO^\dagger + CO^\dagger \tag{22}$$

$$CO^* + CO \rightarrow C + CO_2, \tag{23}$$

correspond to two channels for deexcitation of CO^* by CO. The total rate coefficient is known,[23] but the branching ratio is not. It has been assumed in these calculations that 10% of the $CO^* + CO$ reactions follow the $C + CO_2$ branch. The C production rate is critically dependent upon this branching ratio and there is, unfortunately, no information on the branching ratio or even on the carbon concentrations found in CO discharges. The carbon is readily removed by reaction (44),

$$C + O_2 \rightarrow CO^\dagger + O^* \tag{44}$$

with O_2. This is a satisfactory explanation of the observation that the addition of O_2 to a CO discharge reduces or eliminates carbon deposition in the system. The products of this reaction have been assumed to be $CO^\dagger$ and $O(^1D)$ as these are spin allowed and energetically accessible.

Finally, mention should be made of the possible role of $O(^1D)$ in the discharge. It is rapidly formed by reactions (17), (18), and (28):

$$O_2 + e^- \rightarrow O + O^* + e^-, \tag{17}$$

$$O + e^- \rightarrow O^* + e^-, \tag{18}$$

$$O_2^+ + e^- \rightarrow O + O^*, \tag{28}$$

and, perhaps, (44) as discussed above. The O^* is then rapidly removed in reactions (57) and (58):

$$O^* + CO \rightarrow O + CO^\dagger, \tag{57}$$

$$O^* + CO \rightarrow O + CO. \tag{58}$$

Although O^* has little effect upon the chemistry of the system it may, in this way, be an important source for heating the gas.

Using the reaction rates for both $O(^1D)$ quenching into translational energy [reaction (58)] and relaxation of $CO^\dagger$ into translational energy [reaction (59)] as given in Table III, the total energy flux from these reactions is sufficient to explain the observed[17] gas temperature increase with increasing O_2 pressure beyond the optimum pressure for laser output.

V. HETEROGENEOUS VERSUS HOMOGENEOUS ELECTRON-LOSS PROCESSES

In low-pressure small-diameter laser discharges, ambipolar diffusion can dominate the

electron loss mechanism. Here we consider the competition between homogeneous recombination and ambipolar diffusion in controlling the electron density in a CO-laser system.

In order to estimate the relative contribution to the electron loss rate, the time scale associated with diffusion and recombination must be estimated. The time scale for diffusion loss is found from a solution to the radial diffusion equation as

$$\tau_{diff} = (e/kT_e)(\Lambda^2/\mu_+),$$

where μ_+ is the ion mobility, T_e is the mean electron temperature, and Λ is the characteristic diffusion length ($\Lambda \geq R/2.4$ where R is the tube radius). For a 20-torr, 300-°K plasma in which CO^+ is the dominant ion (taking $R = 1.4$ cm and $T_e = 0.9$ eV)[47]

$$\tau_{diff}^{CO^+} = 5.1^{-4} \text{ sec}.$$

The ambipolar diffusion time for O_2^+ as the dominant ion is only slightly slower than that of CO^+ ($\tau_{diff}^{O_2^+} = 4.7^{-4}$ sec) under the same conditions.[47] Evidence suggests that the diffusion of ion clusters in the case of $C_2O_2^+$ is not substantially different from the parent ion.

The time scale for homogeneous recombination can be estimated from the rate of the recombination reactions, (26) in the case of $C_2O_2^+$, and (27) + (28) in the case of O_2^+. Thus,

$$\tau_{recomb}^{C_2O_2^+} = 4.6^{-4} \text{ sec}$$

and

$$\tau_{recomb}^{O_2^+} = 1.7^{-3} \text{ sec}.$$

These estimates show that the ambipolar loss time scale and the homogeneous recombination time scale are of the same order. At higher-pressure and lower-temperature operation, the homogeneous recombination process will dominate and the calculations presented above on the influence of oxygen in the electron density will more quantitatively apply. Under the conditions of the calculations presented in this study, the quantitative predictions will be reduced, but the substitution of O_2^+ as the dominant ion will still clearly reduce the rate of electron loss and produce a corresponding increase in electron density at constant E/N.

VI. SUMMARY AND CONCLUSION

We have attempted to demonstrate a consistent interpretation to the effects of small amounts of molecular O_2 in a low pressure cw CO-He laser system. The observation that very small amounts of O_2 lead to a reduction in E/N, a reduction in plasma temperature, and an increase in output power we attribute to the emergence of O_2^+ as the dominant positive ion. Since O_2^+ recombines more slowly than CO^+ or its polymers at the E/N of interest, the same current can be maintained by a lower E/N. The reduction in E/N results in a more favorable fraction of the electron energy into vibration with a corresponding decrease of electron energy into CO electronic states. The thermal energy produced by electronic quenching ($E - V/T$) is reduced and the plasma cools. The simultaneous improved vibrational excitation and reduced plasma temperature leads to improved laser energy output.

At higher O_2 additions, the O atoms generated primarily by predissociation of O_2 lead to direct deactivation of the upper vibrational levels of CO responsible for lasing through VT processes as well as increased plasma temperatures through $O(^1D)$ formation by electron impact followed by quenching by CO through $E - V/T$ processes. These two O atom effects lead to a degradation of laser output.

The dynamics of carbon formation and loss is proposed to occur through electronically excited CO, but is not found to be important in the laser dynamics except to influence the laser lifetime. This latter effect occurs when the carbon deposits increase cavity losses such that lasing ceases.

The importance of plasma chemistry processes involving minor constituents attests to the complexity of molecular discharge sustained lasers. The dominance of recombination kinetics as opposed to ionization processes suggests that other additives might enhance laser output in ways previously unappreciated.

Lastly, we would like to remark on the role of superelastic processes in the CO laser system. It is clear that superelastic feedback from the vibrationally excited CO is critical in determining observed ionization rates, and hence electron densities. We would like to suggest that superelastic processes are also responsible for the normal negative E-vs-I characteristics measured in low-temperature CO lasers and for the deviation to a positive E-vs-I characteristic observed under higher-temperature operation. We suggest that without O_2, the E/N of the discharge is high, but that at liquid-N_2 cooling the CO vibrational modes are still sufficiently excited that the superelastic feedback determines the ionization rate and electron density. As the E/N is reduced, a more favorable vibrational excitation by electrons is produced coincident with a reduction in plasma temperature. The subsequent increase in vibrational excitation leads to increased superelastic feedback, greater ionization, and an increased electron density, i.e., current. This behavior

demonstrates a negative E-vs-I characteristic.

Under very high plasma temperatures, such as maintained by Keren *et al.*, the superelastic contribution is minimal. Therefore, the ionization is determined by the high-energy tail of the electron distribution as provided by the E/N. When the E/N is reduced the high-energy tail is depressed leading to reduced ionization rates and lower electron densities, i.e., a reduction in current. This behavior is characterized by a positive E-vs-I characteristic.

It is clear from this suggestion that low-temperature operation or the presence of additives would give negative E-vs-I behavior in agreement with observation. Since the only positive E-vs-I characteristic has been reported under high-temperature operation, we believe this explanation is consistent with available experimental observation.

ACKNOWLEDGMENTS

The major part of this research was supported by Defense Advanced Research Projects Agency through the Office of Naval Research, Boston under Contract No. N00014-75-C-0284. W. L. M. would like to express his appreciation to Dr. A. V. Phelps for helpful discussions on part of this research.

*Present address: Joint Institute for Laboratory Astrophysics, University of Colorado, Boulder, Colo. 80302.

[1]R. E. Hake and A. V. Phelps, Phys. Rev. 158, 70 (1967).
[2]H. Ehrhardt, L. Langhans, E. Liner, and H. S. Taylor, Phys. Rev. 173, 222 (1968).
[3]D. Rapp and D. D. Briglia, J. Chem. Phys. 43, 1480 (1965).
[4]L. J. Kieffer, Joint Institute for Laboratory Astrophysics Report No. 13, 1973 (unpublished).
[5]S. Trajmar, D. C. Cartwright, and W. Williams, Phys. Rev. A 4, 1482 (1971).
[6]C. E. Watson *et al.*, J. Geophys. Res. 72, 3961 (1967).
[7]L. D. Thomas and R. K. Nesbet, Phys. Rev. A 11, 170 (1975).
[8]J. M. Ajello, J. Chem. Phys. 55, 3158 (1971).
[9]S. Chung and C. C. Lin, Phys. Rev. A 8, 2463 (1973).
[10]T. Sawada, D. L. Sellin, and A. E. S. Green, J. Geophys. Res. 77, 4819 (1972).
[11]H. F. Schaefer III and W. H. Miller, J. Chem. Phys. 55, 1107 (1971). This transition is thought to go to the $c\,^1\Sigma_u^-$ state rather than the $A\,^3\Sigma_u^+$ state by S. Trajmar, W. Williams, and A. Kupperman, J. Chem. Phys. 56, 3759 (1972).
[12]P. H. Krupenie, J. Phys. Chem. Ref. Data 1, 423 (1972).
[13]P. D. Burrow, J. Chem. Phys. 59, 4922 (1973).
[14]W. L. Nighan, Phys. Rev. A 2, 1989 (1970).
[15]S. Yarema, M. S. thesis (Wayne State University, 1974) (unpublished).
[16]M. L. Bhaumik, W. B. Lacina, and M. M. Mann, IEEE J. Quantum Electron. 8, 150 (1972).
[17]T. S. Hartwick and J. Walder, IEEE J. Quantum Electron 8, 455 (1972).
[18]H. Keren, P. Avivi, and F. Dothan, IEEE J. Quantum Electron. 11, 590 (1975).
[19]H. Keren, P. Avivi, and F. Dothan, IEEE J. Quantum Electron. 12, 58 (1976).
[20]W. Lowell Morgan and Edward R. Fisher, RIES Report 74-56, Wayne State University, 1974 (unpublished).
[21]T. Keneshea, Air Force Cambridge Research Laboratory, Report No. AFCRL-67-0221, Environmental Paper No. 263, 1967 (unpublished).
[22]D. A. Parkes, Trans. Faraday Soc. 68, 627 (1972).
[23]G. W. Taylor and D. W. Setser, J. Chem. Phys. 58, 4040 (1973).
[24]J. J. Leventhal and L. Friedman, J. Chem. Phys. 46, 997 (1967).
[25]M. Saporoschenko, J. Chem. Phys. 49, 768 (1968).
[26]S. L. Chang and J. L. Franklin, J. Chem. Phys. 54, 1487 (1971).
[27]R. L. Horton, J. L. Franklin, and B. Masseo, J. Chem. Phys. 62, 1739 (1975).
[28]R. E. Center, J. Appl. Phys. 44, 3538 (1973).
[29]J. M. Bardsley and M. A. Biondi, *Advances in Atomic and Molecular Physics*, Vol. 6, edited by D. R. Bates (Academic, New York, 1970).
[30]R. J. Donovan and D. Hussain, Chem. Rev. 70, 489 (1970).
[31]K. Schofield, Planet. Space Sci. 15, 643 (1967).
[32]E. W. McDaniel *et al.*, *Ion-Molecule Reactions* (Wiley-Interscience, New York, 1970).
[33]M. H. Bortner, R. H. Kummler, and T. Baurer, in Defence Nuclear Agency Reaction Rate Handbook, edited by M. H. Bortner and T. Baurer, (DoD Nuclear Information and Analysis Center, Santa Barbara, Calif., 1973), Chap. 24, DNA 1948H, Revision No. 5, 1973 (unpublished).
[34]E. W. McDaniel, *Collision Phenomena in Ionized Gases* (Wiley, New York, 1964).
[35]M. B. McElroy and J. C. McConnell, J. Geophys. Res. 76, 6674 (1971).
[36]R. G. Shortridge and M.C. Lin, J. Chem. Phys. (to be published).
[37]R. E. Center, *Proceedings of the Ninth International Shock Tube Symposium*, edited by D. Bershader and W. Griffith (Stanford University, Stanford, 1973).
[38]F. E. Niles, J. Chem. Phys. 52, 408 (1970).
[39]M. R. Verter and H. Rabitz, J. Chem. Phys. 64, 2939 (1976).
[40]G. Abraham and E. R. Fisher, J. Appl. Phys. 43, 4621 (1972).
[41]R. C. Millikan and D. R. White, J. Chem. Phys. 39, 3209 (1963).
[42]W. L. Nighan and W. J. Wiegand, Phys. Rev. A 10, 922 (1974).
[43]J. F. Prince and A. Garscadden, Appl. Phys. Lett. 27, 13 (1975).
[44]P. Bletzinger *et al.*, IEEE J. Quantum Electron. 11, 317 (1975).
[45]E. R. Fisher and A. J. Lightman, J. Chem. Phys. (to be published).
[46]A. J. Lightman and E. R. Fisher, Appl. Phys. Lett. 29, 593 (1976).
[47]W. Lindinger and D. L. Albritton, J. Chem. Phys. 62, 3517 (1975).
[48]G. Hancock and I. W. M. Smith, Appl. Opt. 10, 1827 (1971).